Hindawi
International Transactions on Electrical Energy Systems
Volume 2022, Article ID 1837800, 13 pages
https://doi.org/10.1155/2022/1837800

Research Article

Intelligent Edge Computing Detection Vehicle and Detection Method Based on Tunnel Lining Concrete

Xiaoming You,[1] Gongxing Yan ,[2] and Zhengqiang Yang[3]

[1]*Chongqing Vocational Institute of Engineering, Chongqing 402260, China*
[2]*College of Architectural Engineering, Luzhou Vocational and Technical College, Luzhou, Sichuan, China*
[3]*Jiangsu Vocational Institute of Architectural Technology, Xuzhou 221116, Jiangsu, China*

Correspondence should be addressed to Gongxing Yan; yxm411@cqvie.edu.cn

Received 21 June 2022; Revised 12 August 2022; Accepted 23 August 2022; Published 10 October 2022

Academic Editor: Raghavan Dhanasekaran

In recent years, with the rapid development of tunnel construction in China, the length of tunnels has continued to increase, and the consequent tunnel disease detection has attracted more and more attention from maintenance departments. Among many diseases, lining cracks are the most common, which directly reflect the stress of the lining, which is very important for the study of tunnel diseases. In view of the current detection status and detection requirements, this article has carried out research work on a vehicle-mounted tunnel lining crack detection system based on image processing. Due to the grayscale difference between the cracks on the lining surface and the lining background, these differences lead to significant crack edge features and relatively stable detection. Therefore, this article designs an intelligent edge algorithm system for cracks on the lining surface to detect the edges of the image, extract the edges of cracks, and remove useless interference information in the lining background. The experiment proves that the paired sample *t*-test can find that after the experiment is over, the *P* value of different edge detection operators for global threshold segmentation is less than 0.05, which has a significant difference. The Canny, Deriche, and Lanser filters are relatively strong, and the extracted crack edge noise is relatively small. Finally, the parameter values of the crack image are calculated, and the calculated values of the crack parameters provide a scientific and reliable basis for tunnel safety evaluation.

1. Introduction

Intelligent edge computing utilizes Internet of Things edge devices for data collection and intelligent analysis and computing, enabling intelligence to flow between the cloud and the edge. As the most basic mode of transportation, the highway has the widest coverage and the strongest service function, providing convenient conditions for the rapid development of China's economy. Due to the changeable terrain of China, the excavation of tunnels has become an important form of construction of the main transportation hub. The acceleration of the national modernization process and the continuous improvement of traffic convenience requirements have prompted a continuous increase in the number of tunnels. The excavation of road tunnels has greatly eased the increasingly serious traffic pressure in the city, reduced the transportation time of passenger and freight transportation, and greatly improved the local economy and living conditions. Inadequate investment in tunnel management and maintenance is the biggest problem facing China's tunnels in recent years. It has not done enough to apply the theoretical knowledge of tunnel management and maintenance to actual inspections, and the early detection of tunnel diseases is insufficient; the tensile strength of concrete itself is very low, so the surface of the concrete structure usually has microcracks, which will not damage the performance of the tunnel.

Some developed countries abroad are more mature and advanced in tunnel lining crack detection technology than domestic ones, but the technology is relatively confidential. The technology is quite mature. Di Carlo F obtained the tunnel lining image by comparing the intensity of the

emitted and received laser signals and compared the phase difference between the emitted and received lasers to obtain the distance between the tunnel lining surface and the track centerline [1]. Based on image analysis technology, Briffaut's has written a program to count the number of pixels in the analysis area selected in the digital photo and the number of pixels in the crack area, calculate the ratio, and calculate the area ratio of the crack area. Parameters such as crack width are obtained [2]. Gao et al. received the electromagnetic wave reflected back to the ground through the receiving antenna. When the electromagnetic wave is propagated in the underground medium, it will be reflected when it encounters the interface with an electrical difference. According to the received electromagnetic wave waveform, amplitude intensity, and time change characteristics, the space of the underground medium is inferred [3].

The application of automatic crack detection technology in China mainly focuses on detecting road pavement cracks. The automatic detection of tunnel lining cracks is still in its infancy. The technology is not very mature, and the application is not very extensive. It is far behind western developed countries and cannot meet the growing number of tunnels. Testing needs: Jiang Y obtained the tunnel lining image and the distance between each point of the tunnel lining surface and the track centerline by analyzing the intensity and phase difference of the transmitted and received laser signals so as to mark the tunnel diseases and calculate the parameters such as crack length and water seepage area [4]. Harada et al. used the Otsu threshold segmentation method based on edge detection to segment the image. This method is effective for detecting cracks in the image. It can well separate the cracks from the background and reduce noise interference [5]. Shalabi used the knowledge of image genetic programming to develop an image filter for identifying cracks. Through iterative filtering of local areas of the image, residual noise is successfully filtered out and unclear cracks are detected. This method can be used on different surfaces for the accurate detection of image cracks [6]. These studies provide technical support for tunnel detection and improve the identification efficiency of tunnel detection systems, but they still lack intelligent technology.

Through analysis of domestic and foreign tunnel lining crack detection algorithms, it is found that although there are various detection algorithms, the algorithms still have big problems in image segmentation and image classification. This article conducts an in-depth study on the impact of the environment on the cracks. After the rain penetrates the cracks, the gray value will become larger and the edges will spread. This also increases the difficulty of image segmentation. In this case, the threshold segmentation method cannot be used directly. Thus, the target area of the crack is separated from the background area well. According to the characteristics of the tunnel lining image, this article uses image processing-related technology to process the tunnel lining image. The background of the tunnel image and the characteristics of the tunnel captured by the image are compared and analyzed by image processing technology, which is beneficial to the analysis of the tunnel situation.

2. Intelligent Edge Computing Detection Vehicle and Detection Method Based on Tunnel Lining Concrete

2.1. Cracks in Tunnel Lining and Their Causes

2.1.1. Types of Tunnel Lining. Tunnel lining refers to a permanent support structure built with reinforced concrete and other materials along the periphery of the tunnel body in order to prevent the deformation or collapse of the tunnel rock formation. Its structure usually consists of three parts: arch ring, side wall, and bottom plate. The arch ring is located on the upper part of the lining, and the side walls are located on both sides of the lining. There are straight side walls and curved side walls. The bottom plate is located at the bottom of the lining [7, 8]. The assembled lining is also called fabricated lining or assembled lining. It comprises the arch ring, standing leg, backing plate, template, etc. The arch ring and the standing leg are connected by bolts, and the backing plate is between the arch ring and the standing leg. For disassembly, the template is laid outside the standing legs and arches. This type of lining has some problems, such as the easy formation of splicing joints and water leakage, so it has not been promoted [9, 10].

2.1.2. Classification and Causes of Tunnel Lining Diseases. Tunnel lining diseases can be divided into many types according to different causes. The more common ones are lining leakage caused by failure of waterproofing and drainage, lining cavities caused by deterioration of lining concrete materials, lining cracks and deformation caused by external force, and lining caused by chemical corrosion, corrosion, surface peeling, etc. In summary, the causes of lining diseases can be divided into the lining material itself, the influence of external factors on the lining, and the level of construction. The quality of the lining material itself determines whether the lining is prone to layering and peeling. Even if the quality of the lining is affected by water leakage, external forces, and other factors, it is difficult to cause disease [11, 12]. The influence of external factors on the lining includes leakage water erosion, chemical corrosion, external force, etc. Among them, the leakage water erosion and chemical corrosion will directly cause the lining to corrode and peel off. The external force mainly comes from the formation pressure, including the deformation pressure and loosening of the formation, pressure, and shrinkage stress. Its size is closely related to many factors, including rock geological conditions and the mechanical properties of surrounding rocks. The level of engineering construction cannot be ignored, and the quality of construction directly affects the quality of the lining. The human factors of the construction personnel during the construction process and the load condition of the construction vehicles during the construction process will cause lining diseases. These diseases not only shorten the service life of the tunnel and affect the appearance of the tunnel but also cause other diseases [13, 14]. They often appear in the initial stages of tunnel deterioration, so they

need to be detected and preventive measures taken as soon as possible before the problem becomes more serious.

2.1.3. Types and Evaluation of Tunnel Lining Cracks

(1) Tunnel Lining Crack Type. The severe weather conditions inside the tunnel lead to different cracks. According to their direction and the relationship with the longitudinal axis of the tunnel, they can be divided into three types: longitudinal, transverse, and oblique cracks [15, 16]. Longitudinal cracks are mostly structural cracks, the most common and the most harmful. They generally extend along the longitudinal axis of the tunnel, parallel to or substantially parallel to the longitudinal axis of the tunnel, and mainly appear in the arched waist or arched shoulder. The second is diagonal cracks, which are structural cracks like longitudinal cracks. The third type of crack is the transverse crack, which is similar to the longitudinal crack, and the longitudinal crack is parallel to the human body. They are often called net-like cracks. They are generally distributed at 30°–45° with the longitudinal axis of the tunnel. The intersection of several diagonal cracks can easily cause the lining to fall off. Lateral cracks are also called hoop cracks, which are mainly caused by factors such as changes in the pressure of the surrounding rock and uneven settlement of the foundation. Most of them occur at the entrance of the tunnel and the intersection of soft and hard rock layers and have little effect on the stability of the tunnel [17, 18].

(2) Classification and Evaluation of Tunnel Lining Cracks. Lining cracks directly affect the normal use of the tunnel. When the cracks first form, they are very subtle, not easy to be observed by the naked eye, and pose little harm to the tunnel [19, 20]. With further development, its hazards to the tunnel became apparent, seriously threatening the personal safety of travelers. The classification method of railway tunnel lining cracks in China's railway code divides them into five grades. This method comprehensively considers the length and width of the cracks, as shown in Table 1.

2.2. Image Processing of Tunnel Lining Cracks

2.2.1. Image Characteristics of Tunnel Lining Cracks. Since the characteristics of the collected images are closely related to the selection of subsequent image processing methods, it is necessary to analyze the characteristics of the collected images first. Ideally, the cracks are darker than the background color, but due to the complex environment in the tunnel, the images collected by the image acquisition system usually contain a lot of noise, which undoubtedly increases the difficulty of later image processing [21, 22]. Generally speaking, the collected images have the following in common:

(1) In the process of image acquisition, due to the movement of the detection vehicle, the size of the camera itself, or the influence of the lens, the collected pictures have a certain degree of distortion

(2) The internal environment of the tunnel is relatively complicated, and there must be certain noise in the collected images of the tunnel lining

(3) The pixels occupied by the cracks in the collected images are smaller than the pixels occupied by the background

(4) The uneven texture of the tunnel lining surface will cause the background color of the collected image to change

Therefore, in the image processing process, the distorted image must be corrected first, then the image must be enhanced, and finally, the crack target is separated from the background through image segmentation.

2.2.2. Distorted Image Correction Technology

(1) Distortion Coefficient Calculation. Distortion coefficient refers to the ratio of the root mean square value of the harmonic components of the voltage or current to the root mean square value of the fundamental wave component. We can describe the lens distortion model memory in many ways. The difference between these descriptions is the type of distortion. The main purpose here is radial distortion, and the distorted image is corrected. The process of solving the distortion coefficient is the key part [23]. Let (x, y) be a point on the distorted image, and the corresponding point after correction is (u, v), then the relationship between these two coordinates can be expressed as follows:

$$\begin{aligned} x &= \sum_{i=0}^{n}\sum_{j=0}^{n-i} a_{ij}u^i v^j, \\ y &= \sum_{i=0}^{n}\sum_{j=0}^{n-i} b_{ij}u^i v^j. \end{aligned} \tag{1}$$

In the above formula, a_{ij} and are correction coefficients, and n is the number of corrections. According to the principle of least squares, the square sum of fitting error ε is the smallest [24], namely, the following:

$$\varepsilon = \sum_{l=1}^{L}\left(x_l - \sum_{i=0}^{n}\sum_{j=0}^{n-i} a_{ij}u^i v^j\right)^2. \tag{2}$$

At the same time, it must meet

$$\frac{\partial \varepsilon}{\partial a_{st}} = 2\sum_{l=1}^{L}\left(x_l - \sum_{i=0}^{n}\sum_{j=0}^{n-i} a_{ij}u^i v^j\right)u_l^s v_l^s = 0. \tag{3}$$

Get

Table 1: Evaluation grade table of tunnel lining cracks.

Rank sequence	Classification level	
Extremely heavy	$L > 10m \cap D > 5mm$	Continuous development and fast
Serious	$5m \le L \le 10m \cap D > 5mm$	May collapse under external force
Heavier	$L < 5m \cap 3mm \le D \le 5mm$	Continuous development and slow changes
Medium	$L < 5m \cap D < 3mm$	The development trend is relatively stable
Slight	$D < 1mm$	No development trend

$$\begin{aligned}\sum_{l=1}^{L}\left(x_l - \sum_{i=0}^{n}\sum_{j=0}^{n-i} a_{ij}u^i v^j\right)u_l^s v_l^s &= \sum_{i=0}^{n}\sum_{j=0}^{n-i} a_{ij}\left(\sum_{l=1}^{L} u_l^{i+s} v_l^{j+t}\right) \\ &= \sum_{l=1}^{L} x_l u_l^s v_l^s, \\ \sum_{l=1}^{L}\left(\sum_{i=0}^{n}\sum_{j=0}^{n-i} b_{ij}u^i v^j\right)u_l^s v_l^s &= \sum_{i=0}^{n}\sum_{j=0}^{n-i} b_{ij}\left(\sum_{l=1}^{L} u_l^{i+s} v_l^{j+t}\right) \\ &= \sum_{l=1}^{L} y_l u_l^s v_l^s.\end{aligned} \tag{4}$$

In the formula, L is the number of control point pairs. $s = 0, 1, 2, \ldots, n$, $t = 0, 1, \ldots, n - s$, $s + t \le n$.

(2) Image Reconstruction. After coordinate transformation, the coordinates in the image are not necessarily integers; that is to say, the coordinates (u, v) of the ideal image point after reconstruction is an integer, but the coordinates of the corresponding point in the distorted image are not necessarily integers [25]. In order to obtain the gray value of this point, the gray value of the surrounding points can be used to further define the gray value of the image point (x, y), that is, gray interpolation, which can be used as the gray value of the ideal image point (u, v).

$$f(i + u, j + v) = (1 - u)(1 - v)f(i, j) + uvf(i + 1, j + 1). \tag{5}$$

(3) Crack Image Enhancement. According to the perceptual characteristics of the human visual system, the image is processed, the useful information in the image is highlighted, and the image suitable for human or machine analysis and processing is obtained, thereby enhancing and improving the visual effect. If the tunnel lining image collected by the image acquisition system is not processed in any way, the image quality is not high, which is not conducive to later image analysis, image feature recognition, and extraction. In order to reduce the difficulty of the later work, it is necessary to improve the quality of the collected images. Image enhancement can achieve this goal. Image enhancement is to improve image quality by reducing or eliminating some uncritical parts of the image and highlighting the key parts of the image, as purposed by [26].

(1) Grayscale transformation method: the grayscale transformation method uses the grayscale transformation function to compare or stretch the grayscale of the image. If the gray value range of a gray image is in the $[0, L - 1]$ interval, and it is normalized, then its histogram can be expressed as follows:

$$p(s_k) = \frac{n_k}{n}, k = 0, 1, \ldots, L - 1. \tag{6}$$

In formula (8), n_k represents the total number of pixels whose gray value is s_k, and n is the total number of pixels in the input image.

(2) Homomorphic filtering method: homomorphic filtering uses a filter function to estimate the low and high frequencies of the image. The low frequency is represented by the illumination component and the high frequency is represented by the reflection component.

$$f(x, y) = i(x, y) \cdot r(x, y), \tag{7}$$

where $f(x, y)$ is the image density, $i(x, y)$ is the illumination component, and $r(x, y)$ is the reflection component.

(3) Gradient domain image enhancement method: the uneven distribution of the image on the gradient is also a manifestation of uneven image illumination. If the image gradient is strong and has a clear structure, it means that the contrast of the image is high. The reduction of the image gradient range can also achieve the compression of the image dynamic range, so the image can be enhanced by changing the image gradient [27]. Use the smooth function to process the image gradient to get the following expression:

$$G(x, y) = \nabla H(x, y) \cdot \phi(x, y). \tag{8}$$

The direction of $G(x, y)$ depends on the direction of ∇H, and the values of $\|\nabla H\|$ and $\phi(x, y)$ determine the size of $G(x, y)$.

(4) Enhancement method based on Retinex theory: retinex theory believes that the color and brightness of objects perceived by the human visual system depend on the reflection characteristics of the surface of the object, and the reflectivity of the object is perceived under different lighting conditions. It is based on the algorithm of illumination compensation. In the Retinex model, the image can be expressed as follows:

$$I(x, y) = L(x, y) \cdot R(x, y). \tag{9}$$

Among them, $I(x, y)$ represents the incident light, which reflects the brightness of the image, and $R(x, y)$ represents the reflection property, which

reflects the internal nature of the image. The principle of the Retinex algorithm is to separate the incident component $L(x, y)$ from the image $I(x, y)$ and minimize its impact on the image [28, 29].

(4) Retinex image enhancement algorithm based on guided filter: assuming that the input image I and the guided filtered output image q have a linear relationship locally, this linear relationship can be expressed by the following formula:

$$q_i = a_k I_i + b_k, \quad \forall i \in \omega_k. \tag{10}$$

Decrease the value of $E\ (a_k, b_k)$:

$$E\left(\min_{a_k, b_k}\right) = \sum_{i=\omega_k} \left(\left(a_k I_i + b_k - p_i\right)^2 + \varepsilon a_k^2 \right). \tag{11}$$

The process of solving the above equation by linear regression is as follows:

$$\begin{aligned} a_k &= \frac{1/\omega \sum_{i=\omega_k} I_i p_i - \mu_k \overline{p_k}}{\sigma_k^2 + \varepsilon}, \\ b_k &= \overline{p_k} - a_k \mu_k, \\ \overline{p_k} &= \frac{1}{|\omega|} \sum_{i \in \omega_k} p_i. \end{aligned} \tag{12}$$

The mean value of the output image in the window of pixels centered at k is denoted by μ_k, the variance is denoted by σ_k^2, $\overline{p_k}$ is the average value of the input image in the window of pixels centered at k, and the number of pixels in the window is denoted by $|\omega|$. Calculate the output value of each window, and average these output values, and then the value of q_i can be calculated [30]:

$$q_i = \frac{1}{|\omega|} \sum_{k:\ i \in \omega_k} a_{kl} + b_k = \overline{a_i} I_i + \overline{b_i}. \tag{13}$$

The following can be drawn:

$$\begin{aligned} \overline{a_i} &= \frac{1}{|\omega|} \sum_{k \in \omega_k} a_k, \\ \overline{b_i} &= \frac{1}{|\omega|} \sum_{k \in \omega_k} b_k. \end{aligned} \tag{14}$$

3. Experimental Design of Intelligent Edge Computing Inspection Vehicle and Inspection Method Based on Tunnel Lining Concrete

3.1. Image Acquisition System Design. Edge computing is a distributed processing and storage architecture by decomposing applications or computing services originally provided by central nodes into several parts. The image acquisition part is composed of an image acquisition card, CCD camera and positioning subsystem, speed sensor, distance sensor, and other equipment. The infrared distance sensor detects when the car approaches the tunnel, turn on the infrared distance sensor. When entering the tunnel, the infrared distance sensor triggers the start of the image acquisition system. When the detection system is started, it is necessary to initialize each module first, including of course the setting of parameters such as the image capture card and CCD camera, and turn on the lighting system [31]. When the detection vehicle leaves the tunnel, the infrared distance sensor gives a corresponding signal, and the image acquisition device is turned off. The speed sensor can coordinate the frequency of the camera to collect image data of the tunnel lining and detect the speed of the vehicle. The flowchart of the image acquisition part is shown in Figure 1.

3.2. Test Subject. There are grayscale differences between the cracks on the lining surface and the lining background. These differences lead to significant edge features of the cracks and are relatively stable in the detection. Therefore, this article designs an intelligent edge algorithm system based on the cracks on the lining surface to perform edge detection on the image to extract crack edges and remove useless interference information in the lining background. The more commonly used edge detection operators include Laplace, Prewitt, Roberts, and Sobel. Due to the overlap between the images to be spliced, each image after block division does not maintain the size of the previous single image. This system uses the common edge detection operators in the Halcon platform and the Canny, Shen, Deriche, and Lanser filters in the edges operator to extract the crack edges. The edges of the cracks were extracted after being detected by Laplace, Prewitt, Robert, and Sobel edge detection operators and subjected to global threshold segmentation processing. The edges of the cracks are extracted after Canny, Shen, Deriche, and Lanser edge detection filters are detected, and global threshold segmentation is performed.

3.3. Experimental Method. After the captured image is image-enhanced, image-segmented, and binarized, the pixel value of the crack area in the image is 1, and the pixel value of the background area in the image is 0. The type of crack in the image is usually judged by projection. The specific process of projection method judgment is as follows:

(1) Determine the coordinate system. The origin of the coordinate is the position of the pixel at the upper left corner of the image.

(2) Project the pixels in the target area to the X-axis and Y-axis directions, respectively, with the X or Y coordinates of the pixel position as the horizontal axis, and the total number of pixels at that position as the

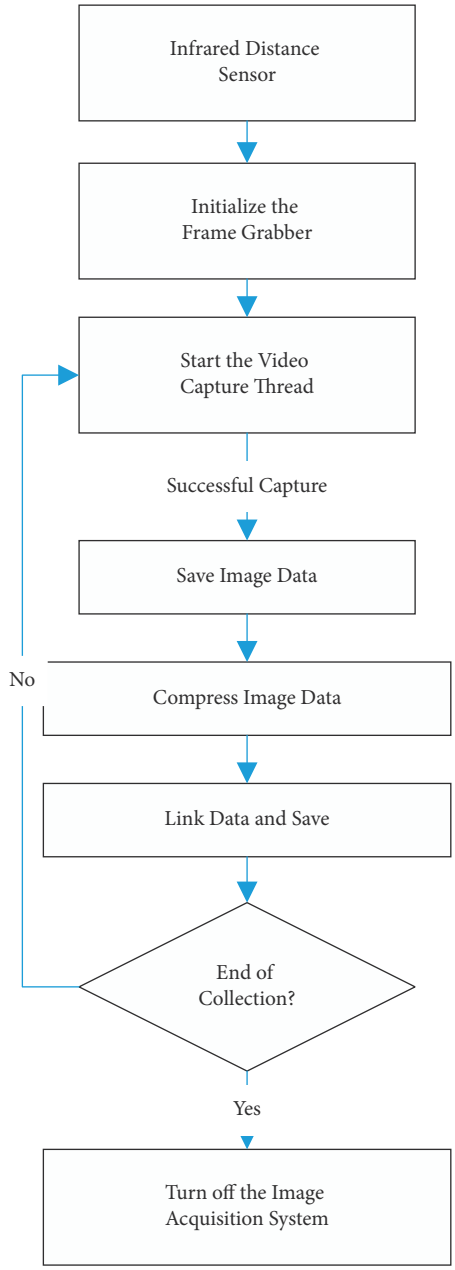

Figure 1: Working principle of system work.

vertical axis, and draw the crack image on this coordinate axis; the drawn image becomes a curved shape.

3.4. Statistical Data Processing Method. SPSS23.0 software was used for data processing, and the count data was expressed as a percentage (%), k is the number of data in this experiment, σ^2 is the variance of all survey results, and $P < 0.05$ indicates that the difference is statistically significant. The formula for calculating reliability is shown in the following:

$$a = \frac{k}{k-1}\left(1 - \frac{\sum \sigma_i^2}{\sigma^2}\right). \quad (15)$$

Table 2: Summary table of reliability test results.

Category	Index combination	Alpha coefficient(α)
Transverse crack	Crack length Crack width Crack area Number of cracks	0.8462
Longitudinal crack	Crack length Crack width Crack area Number of cracks	0.8479
Reticular crack	Crack length Crack width Crack area Number of cracks	0.7653

4. Intelligent Edge Computing Detection Vehicle and Detection Method Based on Tunnel Lining Concrete

4.1. Evaluation Index System Based on Index Reliability Testing. Reliability refers to the stability and reliability of the questionnaire. This article adopts α coefficient method created by L.J. Cronbach. The α coefficient can be obtained by Reliability Analysis in SPSS software. It is generally believed that the α coefficient above 0.8 indicates that the effect of the index setting is very good, and above 0.7 is also acceptable. Here we analyze the reliability of each type of object, and the reliability index we choose for each type of object is slightly different. The results are shown in Table 2.

It can be seen from Table 2 that the data obtained from the four indicators (crack length, crack width, crack area, and number of cracks) for judging the fracture category have an acceptable impact on this experiment ($\alpha > 0.7$). It is necessary to perform image processing on the collected images. This process occupies a pivotal position in the entire image detection process and lays the foundation for the next step.

4.2. Edge Detection Crack Images

4.2.1. Different Threshold Segmentation Methods Combined with Edge Detection Processing Analysis. Global and local threshold segmentation is performed on the image after common edge detection. Compared with the global threshold segmentation method, the local threshold segmentation has a serious blocking effect. The results are shown in Table 3. We make a bar graph based on this result, as shown in Figure 2.

Through the paired sample t-test, it can be found that after the experiment, different threshold segmentation methods combined with edge detection processing resulted in a P value less than 0.05, which has a significant difference. Due to the complexity of tunnel lining cracks, Laplace, Prewitt, Robert, and Sobel edge detection operators cannot meet the requirements of actual testing. They are very sensitive to noise and have a poor processing effect on images with more noise. The detected edges have varying

Table 3: Different threshold segmentation methods combined with edge detection processing data table.

Attributes	Clear	Better	Medium	Blurry	*P*
Laplace + global threshold segmentation	2.44	3.10	3.86	4.83	0.005
Laplace + local threshold segmentation	2.45	3.38	4.49	5.26	0.036
Prewitt + global threshold segmentation	2.22	3.14	3.83	4.72	0.005
Prewitt + local threshold segmentation	2.30	3.34	4.47	4.94	0.032
Robert + global threshold segmentation	2.64	3.13	3.81	4.84	0.005
Robert + local threshold segmentation	2.80	3.35	4.42	5.38	0.031
Sobel + global threshold segmentation	2.50	3.12	4.09	4.88	0.005
Sobel + local threshold segmentation	2.89	3.31	4.36	5.12	0.028

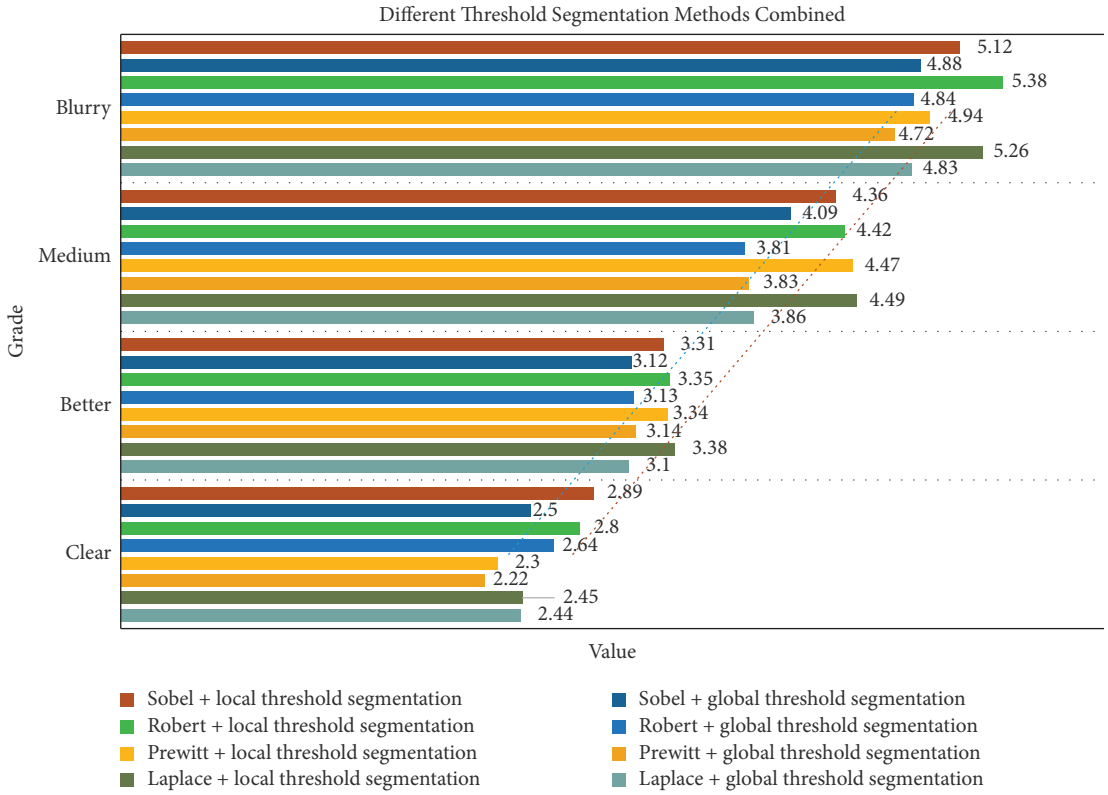

Figure 2: Different threshold segmentation methods combined with an edge detection processing map.

degrees of loss and are not completely connected. The specific situation is shown in Figure 2.

4.2.2. Different Edge Detection Operators Perform Global Threshold Segmentation. We extracted the crack edges from the commonly used edge detection operators, such as Laplace, Prewitt, Robert, Sobel, Canny, Shen, Deriche, and Lanser filters in the edges operator, and then performed global threshold segmentation. The results are shown in Table 4. This result makes a histogram, as shown in Figure 3.

Through the paired sample *t*-test, it can be found that after the end of the experiment, the P value of the global threshold segmentation of different edge detection operators is less than 0.05, which has a significant difference. The Canny, Deriche, and Lanser filters are relatively strong, and the extracted crack edge noise is relatively small. Among them, the noise of the Deriche filter is relatively high. Less, the continuity and integrity are relatively good, closer to the actual fracture edge. The specific situation is shown in Figure 3.

4.2.3. Different Threshold Segmentation Methods for Image Processing and Analysis. The local threshold segmentation method, based on the local characteristics of the image, sets up a mask with the target pixel as the center and determines the threshold according to the local grayscale mean and standard deviation of the pixels in the mask to achieve segmentation. The results are shown in Table 5. Make a combination diagram, as shown in Figure 4.

Through the paired sample *t*-test, it can be found that after the end of the experiment, the P value of the image processed by different threshold segmentation methods is less than 0.05. There is a significant difference. The image after the traditional fixed threshold segmentation has the crack

Table 4: Different edge detection operators perform global threshold segmentation data table.

Attributes	Clear	Better	Medium	Blurry	P
Laplace + threshold segmentation	2.83	2.91	3.92	5.06	0.010
Prewitt + threshold segmentation	3.07	3.89	5.34	4.8	0.010
Robert + threshold segmentation	3.88	5.37	5.32	6.94	0.010
Sobel + threshold segmentation	5.11	5.07	7.36	8.43	0.010
Canny + threshold segmentation	4.91	5.4	7.27	8.6	0.010
Shen + threshold segmentation	5.2	4.99	7.14	8.44	0.010
Deriche + threshold segmentation	5.19	5.04	7.02	8.18	0.010
Lanser + threshold segmentation	4.85	7.31	8.48	9.7	0.010

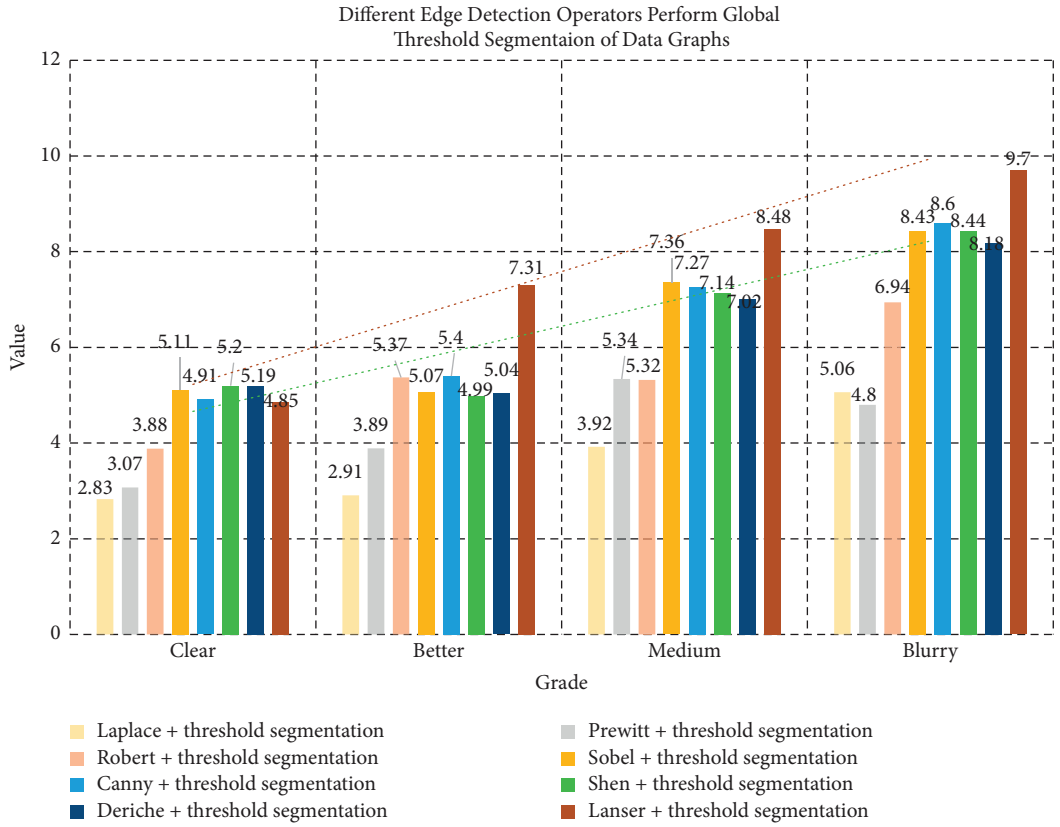

Figure 3: Different edge detection operators perform global threshold segmentation of data graphs.

Table 5: Different threshold segmentation methods to process the image data table.

Attributes	A	B	C	D	E	F	P
Image after image preprocessing	2.20	2.12	3.42	3.97	5.24	5.21	0.001
Fixed threshold segmentation	2.02	2.22	2.94	3.87	5.24	4.95	0.005
Otsu threshold segmentation	1.77	2.69	2.81	4.08	5.43	5.16	0.005
Iterative threshold segmentation	2.17	2.05	3.74	3.42	5.68	5.55	0.001
Maximum entropy threshold segmentation	2.50	2.50	3.23	3.87	4.96	5.40	0.017
Local threshold segmentation	2.32	1.91	3.01	4.62	5.21	5.02	0.028

characteristics submerged in the background. The cracks are well separated from the lining background; after the Otsu threshold segmentation, there are many burrs on the edges of the cracks and there are certain noises, which affect the subsequent identification of the cracks; the iterative threshold segmentation and maximum entropy threshold segmentation have obvious crack characteristics and edge burrs and noise is suppressed; the segmentation speed of local threshold segmentation is slow, which is not conducive to the actual detection needs. By comparing iterative threshold segmentation

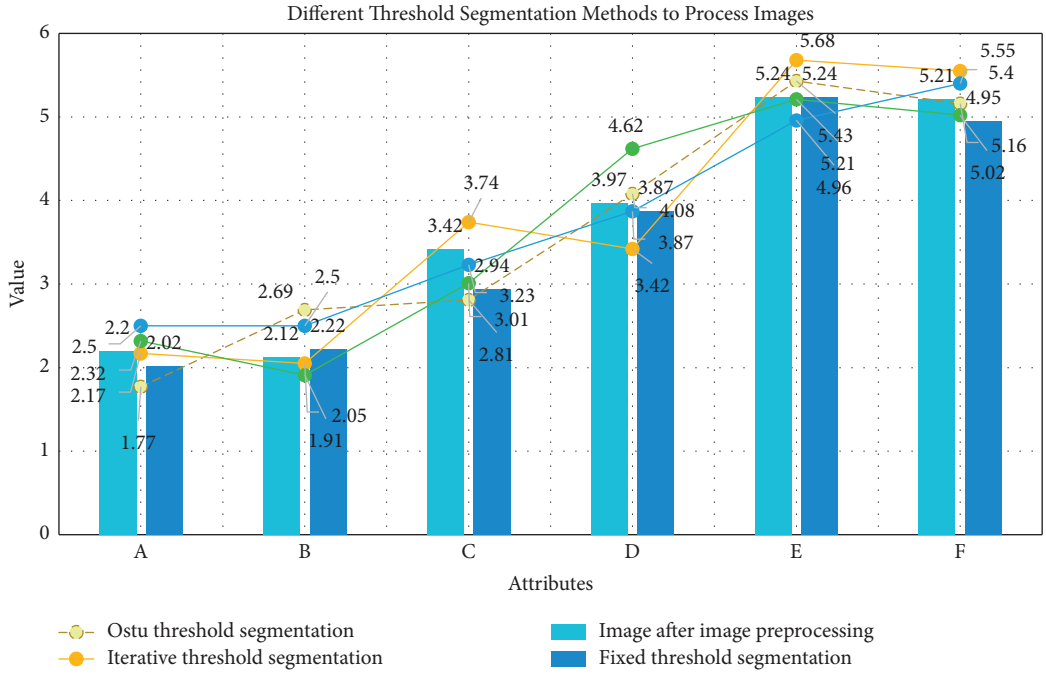

Figure 4: Different threshold segmentation methods to process images.

Table 6: Result data table of crack level detected by the system.

Groups	Extremely heavy(AA)	Serious (%) (A)	Heavier (%) (B)	Heavier (%) (C)	Slight (%) (D)
A (%)	0	9.75	15.42	29.67	45.16
B	0.5	8.3	13.75	34.51	42.94
C	1.9	12.1	22.2	34.12	29.68
D	5	19.5	27.42	31	16.08
E	2	12.7	24.37	37.42	23.51
F	0	4.25	10.64	36.17	48.94

and maximum entropy threshold segmentation, it is found that the maximum entropy segmentation method, as a global segmentation method, has high segmentation efficiency, and the effect is significant, with fewer glitches and noise than iterative threshold segmentation. The specific situation is shown in Figure 4.

4.3. Detectiontunnel Lining Cracks

4.3.1. Analysis of the Results of Crack Levels Detected by the System. The cracks in the lining directly affect the normal use of the tunnel. The cracks are very subtle when they first form and are not easy to be observed by the naked eye, and they pose little harm to the tunnel. The results are shown in Table 6. Based on this result, we make a doughnut chart, as shown in Figure 5.

From Figure 5, we can draw the conclusion that serious lining cracks in the tunnel accounted for 9.75%, heavier lining cracks accounted for 15.42%, medium lining cracks accounted for 29.67%, and slight lining cracks accounted for 45.16%. Based on the above analysis, the tunnel maintenance personnel need to maintain the tunnel in time.

4.3.2. Comparative Analysis of Crack Width Detected by Different Methods. Assuming that the manually detected crack data is the real data, taking the crack width as an example, the comparison result of the partial crack width detected by this system and the manually detected crack width is shown in Table 7.

It can be seen from Table 7 that the crack width detected by this system has a little deviation from the crack width detected manually, and the two are relatively close. It is worth noting that the crack width value detected by this system is generally lower than the value of the crack width detected manually. This is because manual detection is greatly affected by humans, and there is a certain error, which will eventually lead to a large detection result.

Assuming that the number of manually detected cracks is real data, Table 8 is the accuracy of identifying the type of

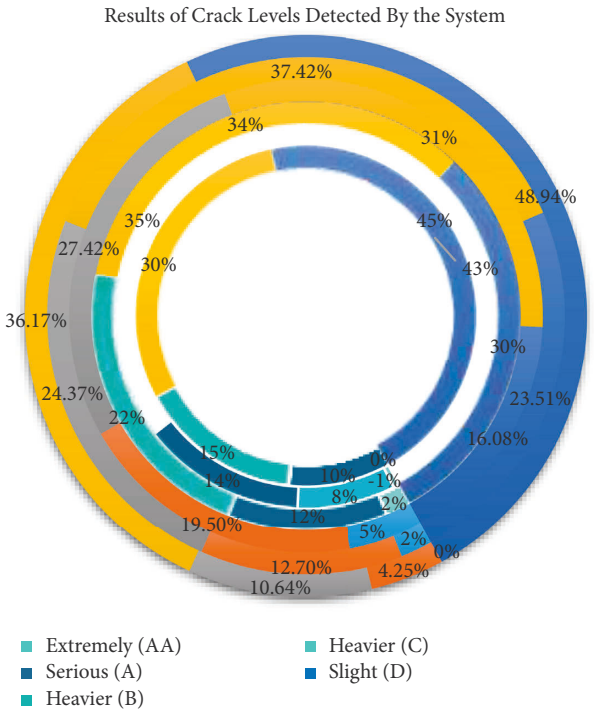

Figure 5: Results of crack levels detected by the system.

Table 7: Comparison result data table of crack width detected by different methods.

Groups	The maximum width of the crack measured by the system	Maximum width of cracks measured manually	Deviation	Accuracy (%)
A	2.08	1.92	0.16	7.69
B	1.94	2.12	0.18	9.28
C	2.22	2.37	0.15	6.76
D	2.45	2.88	0.43	17.55
E	1.81	1.93	0.12	6.63
F	2.50	2.72	0.22	8.80
G	2.40	2.53	0.13	5.42
H	2	2.24	0.24	12.00

Table 8: Data table of the accuracy of the crack type identified by the system.

Crack type	Number of cracks measured by the system	Number of cracks measured manually (A)	Number of cracks measured manually (B)	Number of cracks measured manually (C)	Number of cracks measured manually (D)
Transverse crack	18	21	18	22	15
Longitudinal crack	16	19	18	16	16
Diagonal crack	5	5	8	7	9
Reticular crack	8	9	9	11	16

tunnel cracks detected by this system. We make a pie chart based on this result, as shown in Figure 6.

The correct rate of using this system to detect the type of tunnel lining cracks has reached more than 80%, which meets the design requirements of the system. Due to the definition between longitudinal cracks and oblique cracks, and between oblique cracks and net-like cracks, different workers have large gaps in testing, and there are certain errors, which will eventually lead to large detection results. However, this does not affect the correct judgment of the

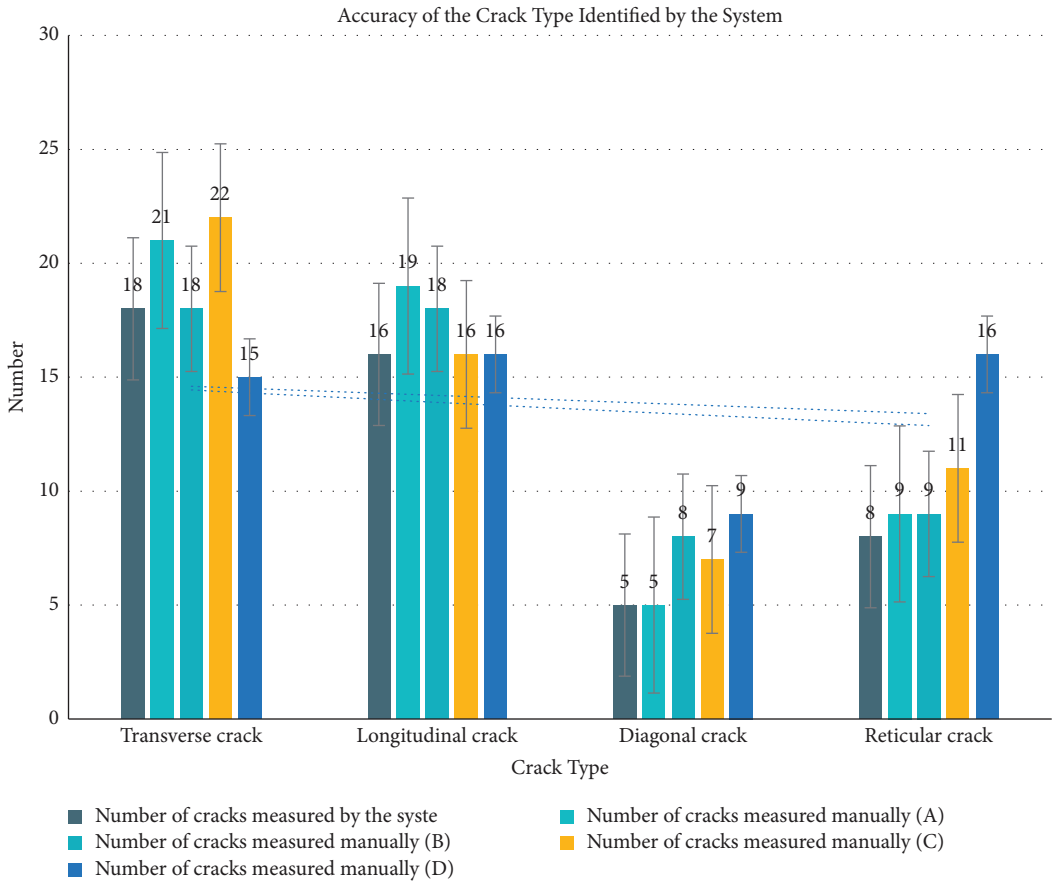

Figure 6: The result of the accuracy of the crack type identified by the system.

system to detect the type of tunnel lining cracks. The specific situation is shown in Figure 6.

5. Conclusions

With the acceleration of the national modernization process, the demand for fast transportation has increased year by year, and the tunnel has gradually become an important transportation hub. However, with the continuous increase of tunnels, tunnel diseases have begun to emerge, and the types of diseases are diverse and cracks appeared due to the lack of prudence of the survey team, insufficient technical force or lack of experience, poor quality of concrete materials, or wrong use of construction personnel, so it is necessary to increase the detection of highway tunnels. However, the current detection technology of tunnel lining diseases in China is still relatively backward, and it is far from meeting the standard requirements of tunnel detection. Therefore, this article designs and studies the automatic crack detection system. In-depth research has been conducted on the development status. China is still relatively backward in tunnel lining crack detection technology, and it is necessary to strengthen the research on tunnel lining crack detection. This article deeply analyzes the types, hazards, and causes of cracks, which shows that it has great practical significance for the research on the detection of tunnel lining cracks. Based on the consideration of the tunnel environment and the characteristics of the tunnel lining crack image, the detection system is designed and researched. The automatic detection system for tunnel lining cracks is overall designed. The detection system is mainly divided into two parts: image acquisition and image processing.

The quality inspection method of tunnel concrete lining has an irreplaceable influence on the quality of tunnel engineering. Therefore, the inspectors need to grasp the key of the tunnel concrete lining quality inspection method so as to improve the actual level of tunnel concrete lining quality through the flexible application of the inspection method on this basis. This article analyzes the working process of the detection system and studies the working principles of each part of the system. The crack detection system first stores the collected images in the industrial computer and then uses the corresponding algorithm to process the images. This article uses a combination of the projection method and threshold method to identify features of processed images. Then, the cracks were spliced, and finally, the characteristics of the cracks in the image were extracted according to the corresponding algorithm; that is, the parameter values of the crack image were calculated, including the length and width of the regular cracks and the area of the irregular cracks. The tunnel is scientifically evaluated based on the calculated parameter values.

This system uses traditional image processing to detect and recognize tunnel lining cracks. Although a lot of improvements have been made in the algorithm, it still has limitations. The crack recognition effect is not as good as the algorithm based on pattern recognition and deep learning. Pattern recognition and deep learning algorithms realize the automatic classification of cracks by training crack samples. This method has a good effect and high accuracy and can identify various cracks. The grayscale features of the cracks and the lining background are relatively close, and the lining surface has a complex grayscale and there are many interferences. Although this system uses effective algorithms for targeted processing, it still inevitably causes some cracks to be removed along with noise, and the unclear cracks on the lining surface are easily overlooked and cannot be detected.

Data Availability

The data that support the findings of this study are available from the corresponding author upon reasonable request.

Conflicts of Interest

The authors declare that they have no conflicts of interest.

Acknowledgments

This work was supported by the General Project of the Chongqing Natural Science Foundation: "structural safety research of large city underwater shield tunnel" (cstc2020jcyj-msxmx0846).

References

[1] F. Di Carlo, A. Meda, and Z. Rinaldi, "Design procedure of precast fiber reinforced concrete segments for tunnel lining construction," *Structural Concrete*, vol. 17, no. 5, pp. 747–759, 2016.

[2] M. Briffaut, F. Benboudjema, and L. D'Aloia, "Effect of fibres on early age cracking of concrete tunnel lining. Part II: numerical simulations," *Tunnelling and Underground Space Technology*, vol. 59, no. oct, pp. 221–229, 2016.

[3] Y. Gao, Y. Jiang, and B. Li, "Voids delineation behind tunnel lining based on the vibration intensity of microtremors," *Tunnelling and Underground Space Technology incorporating Trenchless Technology Research*, vol. 51, pp. 338–345, 2016.

[4] Y. Gao, Y. Jiang, and Y. Du, "Vibration analysis of mountain tunnel lining built with forepoling method," *Smart Structures and Systems*, vol. 21, no. 5, pp. 583–590, 2018.

[5] S. Harada, T. Maeda, and M Moriuchi, "Influence of form covered with sheet on surface quality of tunnel lining concrete," *Doboku Gakkai Ronbunshu F*, vol. 72, no. 2, pp. 76–81, 2016.

[6] F. I. Shalabi, E. J. Cording, and S. L. Paul, "Sealant behavior of gasketed segmental tunnel lining – conceptual model," *Geomechanics and Tunnelling*, vol. 9, no. 4, pp. 345–355, 2016.

[7] O. S Bursi, T Nicola, and F Manuel, "Structural monitoring for the cyclic behaviour of concrete tunnel lining sections using FBG sensors," *Structural Control and Health Monitoring*, vol. 23, no. 4, pp. 749–763, 2016.

[8] S Nakamura, A Yamashita, and F Inoue, "Inspection test of a tunnel with an inspection vehicle for tunnel lining concrete," *Journal of Robotics and Mechatronics*, vol. 31, no. 6, pp. 762–771, 2019.

[9] H Chu, X Yang, H Ye et al., "Experimental study on blasting damage accumulation law of tunnel lining concrete," *Tiedao Xuebao/Journal of the China Railway Society*, vol. 40, no. 3, pp. 132–136, 2018.

[10] Z Yang, X Guoqiang, and Z Liming, "Simulation of tunnel lining concrete quality radar detection based on FDTD & its application analysis," *Wu Tan Hua Tan Ji Suan Ji Shu*, vol. 39, no. 4, pp. 430–438, 2017.

[11] X. Guang and G. -C. Tang, "Analysis of sulphate attack on tunnel lining concrete in actual railway line of southwest China with epma," *Oxidation Communications*, vol. 39, no. 2, pp. 1440–1451, 2016.

[12] K. Takahashi, T. Oyamada, and S. Hanehara, "Mix proportions of tunnel lining concrete in consideration of the resistance of scaling," *Cement ence & Concrete Technology*, vol. 70, no. 1, pp. 378–383, 2016.

[13] X Chen, Q Shi, and L. Yang, "ThriftyEdge: resource-efficient edge computing for intelligent IoT applications," *IEEE Network*, vol. 32, no. 1, pp. 61–65, 2018.

[14] R. Dautov, S. Distefano, and D. Bruneo, "Metropolitan intelligent surveillance systems for urban areas by harnessing IoT and edge computing paradigms," *Software: Practice and Experience*, vol. 48, no. 8, pp. 1475–1492, 2018.

[15] T. Wang, Y. Liang, and Y. Yang, "An intelligent edge-computing-based method to counter coupling problems in cyber-physical systems," *IEEE Network*, vol. 34, no. 3, pp. 16–22, 2020.

[16] Z. Wang, "Joint time delay and energy optimization with intelligent overclocking in edge computing," *Ence China(Information Ences)*, vol. 63, no. 4, pp. 154–169, 2020.

[17] A. Abraham, P. K Muhuri, and A. K. Muda, "Advances in Intelligent Systems and Computing] Hybrid Intelligent Systems," *Edge detection for cement images based on interactive genetic algorithm*, vol. 734, pp. 41–50, 2018.

[18] Y. D. O. N. G. Tu, "Key technologies and application of edge computing," *ZTE Communications*, vol. 2, no. 15, pp. 30–38, 2017.

[19] S. Chen, H. Wen, and J. Wu, "Internet of things based smart grids supported by intelligent edge computing," *IEEE Access*, vol. 7, no. 1, pp. 74089–74102, 2019.

[20] T. Wang, Y. Liang, and Y. Yang, "An intelligent edge-computing-based method to counter coupling problems in cyber-physical systems," *IEEE Network*, vol. 34, no. 3, pp. 16–22, 2020.

[21] B. Cao, L. Zhang, and Y. Li, "Intelligent offloading in multi-access edge computing: a state-of-the-art review and framework," *IEEE Communications Magazine*, vol. 57, no. 3, pp. 56–62, 2019.

[22] H. Qiu, M. Qiu, and R. Lu, "Secure V2X communication network based on intelligent PKI and edge computing," *IEEE Network*, vol. 34, no. 2, pp. 172–178, 2020.

[23] H. Guo, J. Liu, and J. Ren, "Intelligent task offloading in vehicular edge computing networks," *IEEE Wireless Communications*, vol. 27, no. 4, pp. 126–132, 2020.

[24] S. H. Han, M. S. Cho, and Y. K. Yu, "A study on cantilever deformation inspection method using image processing," *The Transactions of the Korean Institute of Electrical Engineers*, vol. 66, no. 6, pp. 988–994, 2017.

[25] G. Zhao, "Research on inspection method of dynamic load of truck by using EWT," *International Journal of Information Systems and Supply Chain Management*, vol. 11, no. 1, pp. 49–64, 2018.

[26] V. N. Nguyen, R. Jenssen, and D. Roverso, "Automatic autonomous vision-based power line inspection: a review of current status and the potential role of deep learning," *International Journal of Electrical Power & Energy Systems*, vol. 99, pp. 107–120, 2018.

[27] D. Yang, R. Hirose, and R. Shigeo, "Development of a stable localized visual inspection system for underwater structures," *Advanced Robotics*, vol. 30, no. 21, pp. 1415–1429, 2016.

[28] W. Sui, Z. Zhu, and G. Cao, "Dynamic responses of axially moving telescopic mechanism for truss structure bridge inspection vehicle under moving mass," *Journal of Vibroengineering*, vol. 18, no. 1, pp. 408–416, 2016.

[29] B. Ju, H. Zhu, and J. Xu, "Rail contour matching method based on random vibrations of a rail inspection vehicle," *Zhendong Yu Chongji/journal of Vibration & Shock*, vol. 36, no. 3, pp. 65–69, 2017.

[30] A. Hallawa, G. Iacca, and C. Sariman, "Morphological evolution for pipe inspection using Robot Operating System (ROS)," *Materials and Manufacturing Processes*, vol. 35, no. 6, pp. 714–724, 2020.

[31] Y. Zhou, *Image Recognition Algorithm of Complex Cracks in Metro Tunnel Based on Neural Network*, , pp. 1109–1119, IEEE 2nd International Conference on Electronic Technology, Communication and Information (ICETCI), 2022.